3.2.4 Fabrication and measurement results for the antipodal Vivaldi antenna

Based on the antenna dimensions (Table 3.2) tuned by the HFSS simulation, the antenna has been carved for UWB usage from a copper coated FR4 board. A photograph of the fabricated antenna is shown in Fig. 3.16. The measurements are executed by Agilent E8361A network analyzer in an anechoic chamber and compared with the corresponding simulated values. Figure 3.17 presents the measured and simulated $|S_{11}|$ from 2 to 15 GHz. The measured line closely resembles the simulated one. This design exhibits low $|S_{11}| \leq -10$ dB for the UWB application range. As seen in Fig. 3.18, the actual gain of the antenna is high and nearly constant (7 dB) in the UWB range. Figures 3.19 show the far-field radiation patterns of the proposed antenna in H and E planes at 5 and 7 GHz. Co- and Cross-polarizations are also included. From these figures, it is found that the measured radiation patterns agree well with simulated ones. In addition, the cross polarization levels in the maximum radiation direction are investigated and shown in Fig. 3.20. The proposed antenna has a good cross polarization level (less than -15 dB).
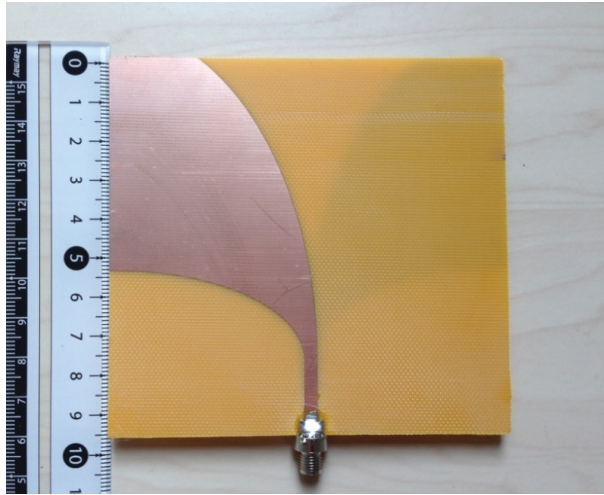

Figure 3.16: Fabricated antipodal Vivaldi antenna

Another important parameter for an antenna operating in UWB systems is group delay. Since group delay is calculated as the rate of change of the total phase shift with respect to angular frequency, this parameter has an influence upon the system performance. The larger group delay variation would cause more signal distortion. Figure 3.21 shows the group delay of the proposed antenna. Two identical Vivaldi antennas are placed face to face to measure the group delay at distance of 300 mm. As presented in Fig. 3.21 (a), the proposed antenna shows almost constant group delay from 2 to 15 GHz. From Fig. 3.21 (b), one can estimate that the group delay variation is less than ± 0.2 ns in the UWB range. This result indicates that the transmitted signal will not be distorted by

this antenna. Difference from the simulation results may come from the connection loss at the SMA connector as well as the dispersive nature of the electric property of the FR4 substrate. The antenna performance has been compared with previous antipodal Vivaldi antennas in Table 3.4. This table contains important characteristics of UWB antennas. The proposed antenna shows constant group delay, flat gain and good cross-polarization levels at the designed UWB range to compare with the previous ones.
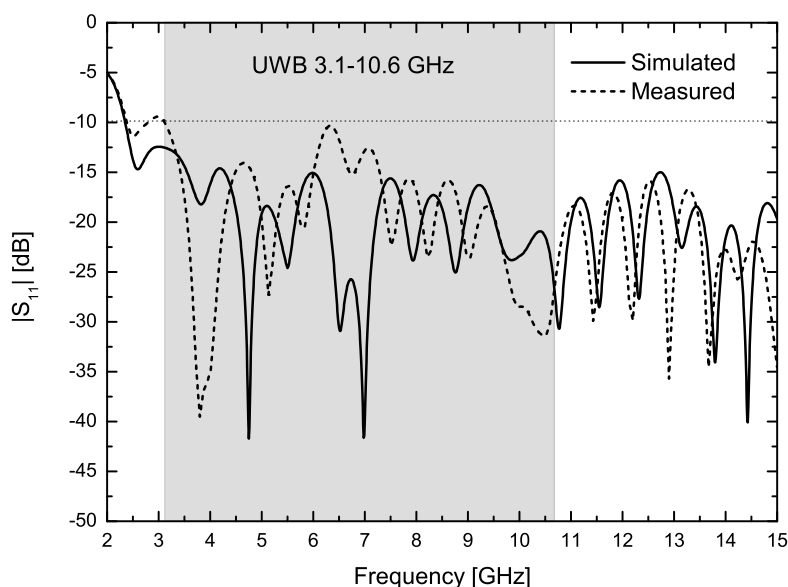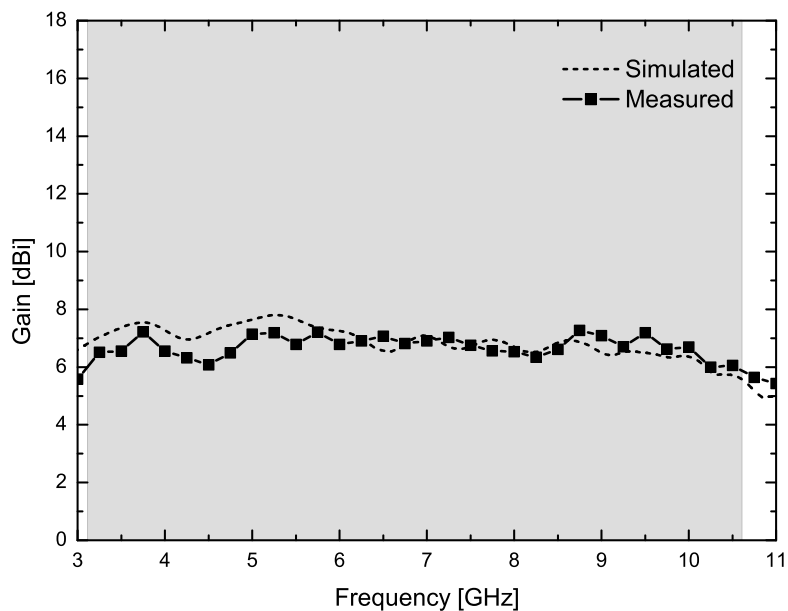

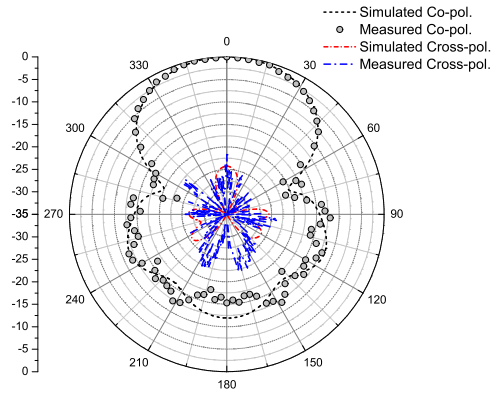
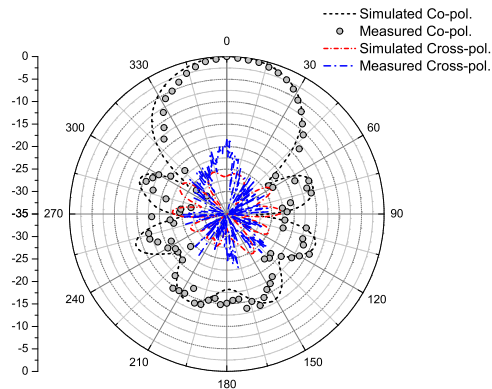Figure 3.17: $|S_{11}|$ of the fabricated antenna
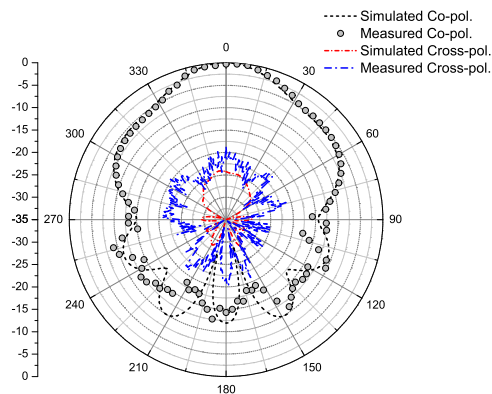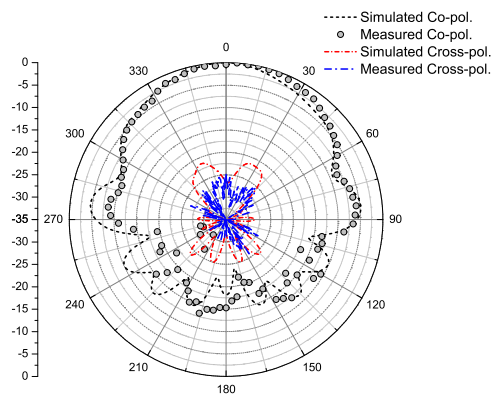

Figure 3.18: Gain of the fabricated antenna

Figure 3.19: Far-field radiation patterns of the proposed antenna. H-plane radiation patterns at (a) 5 GHz, (b) 7 GHz. E-plane radiation patterns at (c) 5 GHz, (d) 7 GHz
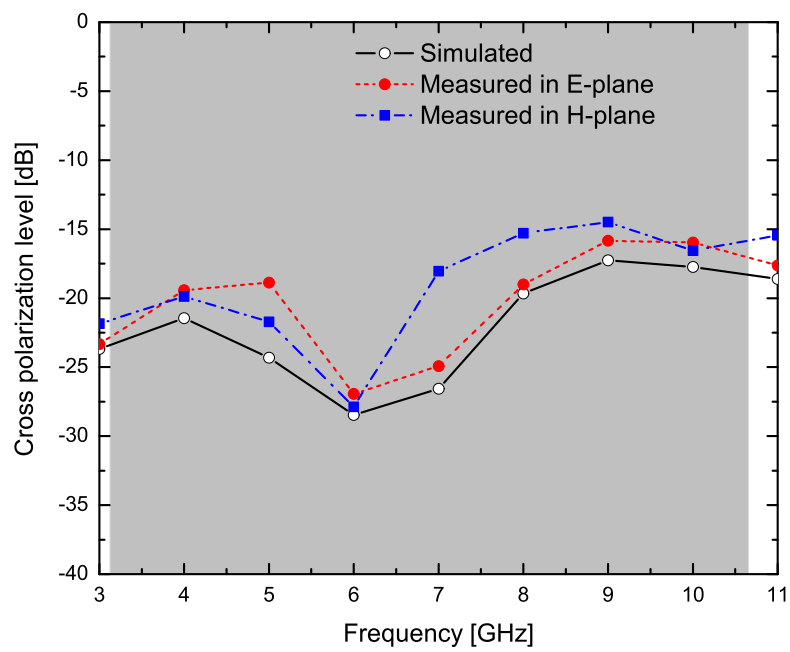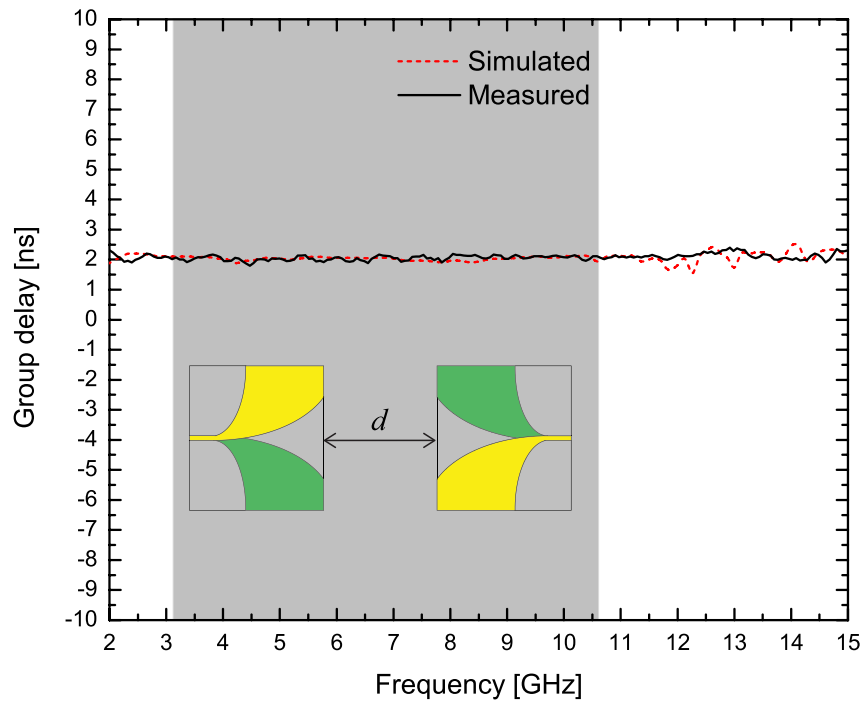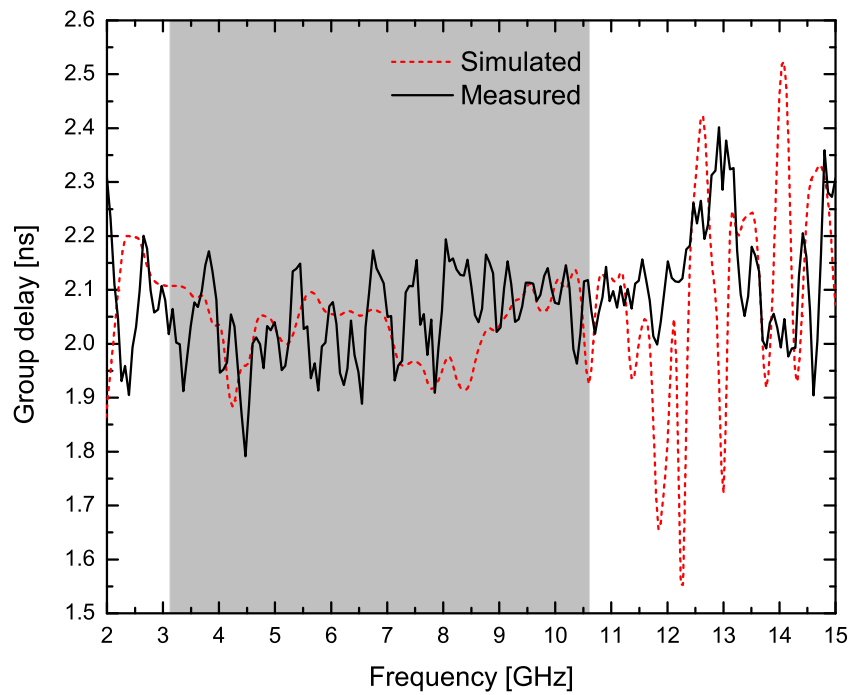
Figure 3.20: Cross polarization levels of the maximum radiation direction

(a)

(b)

Figure 3.21: Group delay at different scales. $d = 300$ mm

Table 3.4: Comparison with previous antipodal Vivaldi antennas

Refs.	Size (mm^2)	Dielectric substrate	Flare design	Feeding line	Low freq. end f_-	Gain in UWB	Cross pol. level	Group delay in UWB
Ours Fig.3.16	100×95.0	FR4, ε_r=4.4, h=1.6 mm	Elliptical	Twin lines	2.36 GHz	Nearly flat 7 dBi	< -15 dB	Nearly constant ±0.2 ns variation
Ref.[52] Fig.1	25.4×67.0	RT/Duroid 5880, ε_r=2.2, h=0.381 mm	Exponential	Microstrip line	8 GHz	5~10 dBi	< -12 dB	N/A
Ref.[53] Fig.1(b)	75.0×105	h=1.5 mm	Exponential	Twin lines	3 GHz	N/A	< -15 dB	N/A
Ref.[54] Fig.1	80.0×80.0	Rogers RO4003, ε_r=3.38, h=0.813 mm	Elliptical, Semi-circle	Microstrip line	2.35 GHz	4~8 dBi	< -20 dB	Large variation
Ref.[56] Fig.3	31.2×45.0	Rogers RO4003, ε_r=3.55, h=0.813 mm	Exponential, Back plane	Microstrip line	6 GHz	Nearly flat 7~8 dBi	< -20 dB	Nearly constant ±1.1 ns
Ref.[57] Fig.1	42.0×120	ε_r=3.3, h=0.8 mm	Fermi-Dirac taper, Slot corrugation at antenna edge	Microstrip line	5.76 GHz	2~10 dBi	< -15 dB	N/A
Ref.[58] Fig.3(b)	64.0×60.0	Rogers Duroid 5880, ε_r=2.3, h=0.254 mm	Exponential and circular, Slot loaded	Microstrip line	4 GHz	1~7 dBi	Max. is −15 dB	N/A
Ref.[60] Fig.1(c)	50.0×66.4	ε_r=4.5, h=1 mm	Exponential, Slot corrugation at antenna edge	Microstrip line	4 GHz	5~8 dBi	N/A	N/A
Ref.[71] Fig.1(c)	48.0×60.0	FR4, ε_r=4.6, h=1mm	Exponential, Slot corrugation at antenna edge	Microstrip line	2.4 GHz	3.7~10 dBi	N/A	Nearly constant ±1.0 ns variation
Ref.[72] Fig.1(b)	36.3×59.8	Rogers RO3206, ε_r=6.15, h=0.64 mm	Exponential, Exponential slot at antenna edge	Microstrip line	5.08 GHz	4~9 dBi	N/A	Large variation ±2.5 ns
Ref.[74] Fig.2(a)	22.0×40.0	Rogers RT6010, ε_r=10.2, h=0.635 mm	Elliptical, Slot corrugation at antenna edge	Microstrip line	4.70 GHz	2.8~5.7 dBi	N/A	Nearly constant ±1.4 ns variation
Ref.[75] Fig.2	59.6×59.9	Rogers RT6010, ε_r=10.2, h=0.64 mm	Elliptical	Microstrip line	2.75 GHz	3.5~9.4 dBi	N/A	N/A

3.2.5 Zero-index metamaterial (ZIM) unit cell for improving gain of the antipodal Vivaldi antenna

a. ZIM unit cell design

Recently, some kinds of ZIM unit cell has been introduced in Refs. [82, 83, 84]. A somewhat different ZIM unit cell configuration is shown in Fig. 3.22. The proposed ZIM unit cell has symmetric structure and been design on the low-cost FR4 substrate with the same substrate parameters which used to design the antipodal Vivaldi antenna in Section 3.2.2. The dimensions of the proposed unit cell is presented in Table 3.5.

The ZIM unit cell is simulated by HFSS 14. Then the characteristics of the ZIM unit cell are calculated from HFSS simulated S-parameters by using the method in Section 3.1.3. In addition, different polarizations are imposed and analyzed for the consideration of anisotropic metamaterials. The first case is when a wave propagation is along y direction and the electric polarization is in x direction. The second case is when a wave propagation is along x direction and the electric polarization is in y direction. As can be seen from Fig. 3.23, S_{11} small than -10 dB for whole UWB from 3.1 to 10.6 GHz. Therefore, wave propagation can pass with a low loss in along y direction.

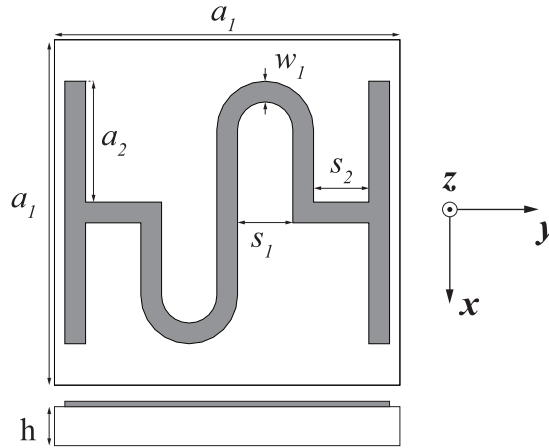Figure 3.22: The proposed ZIM unit cell

Table 3.5: The dimensions of the proposed unit cell

Parameter	Dimension
a_1	5.00 mm
a_2	1.75 mm
w_1	0.30 mm
s_1	0.80 mm
s_2	0.80 mm
h	1.60 mm

88

The effective characteristics of the proposed ZIM unit cell along this direction are plotted in Fig. 3.25. The unit cell exhibits positive refractive index, permittivity and permeability as a normal material.

Figure 3.24 show the simulated S-parameter for the second case. A broad stop-band from 4.1 to 7.5 GHz can be observed in this figure. In x direction, the unit cell shows nearly zero refractive index from 6.1 to 8.3 GHz and negative permittivity from 5.0 to 8.3 GHz in Fig. 3.26. The different between wave propagation along y direction and x direction presents anisotropic metamaterial characteristic of the designed unit cell.

Figure 3.23: Simulated S-parameters of the ZIM unit cell for the first case.

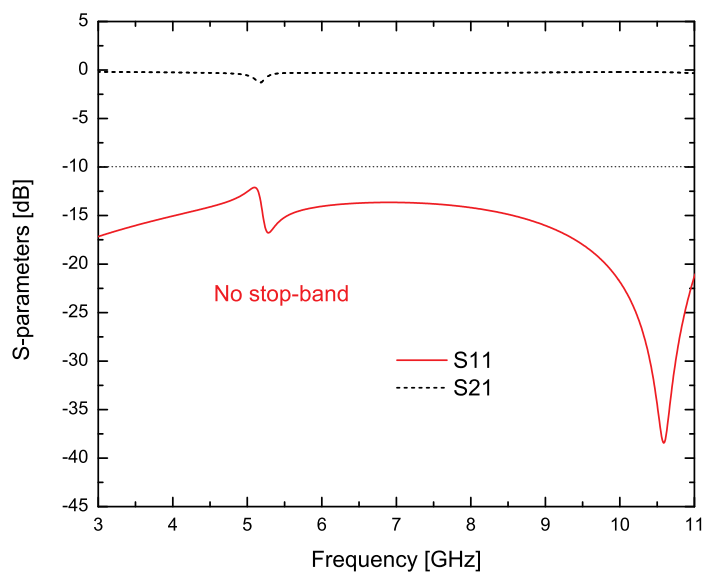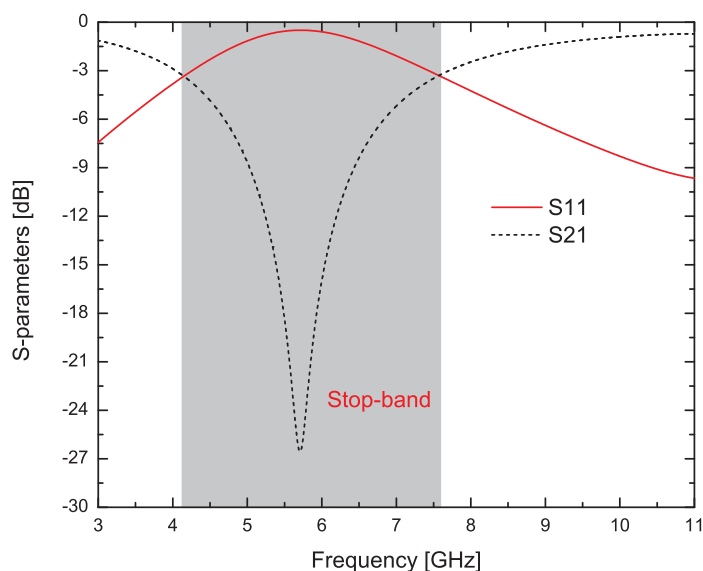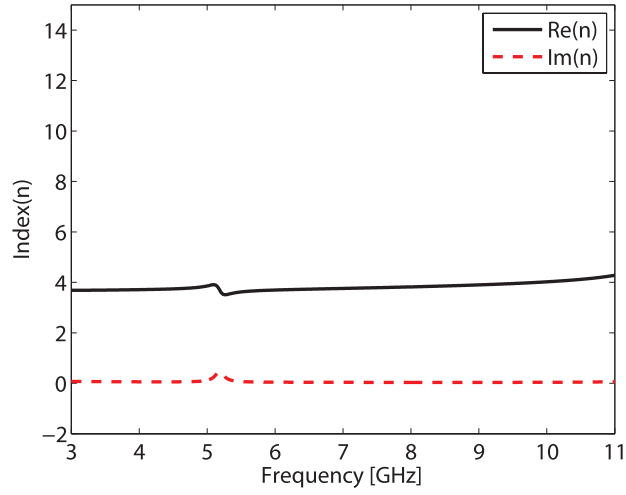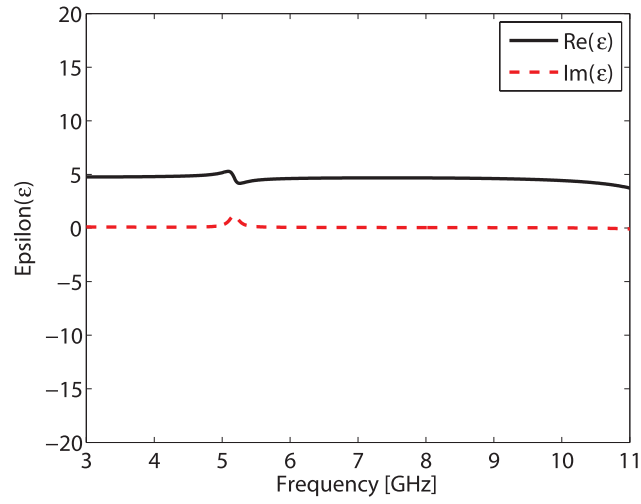Figure 3.24: Simulated S-parameters of the ZIM unit cell for the second case.
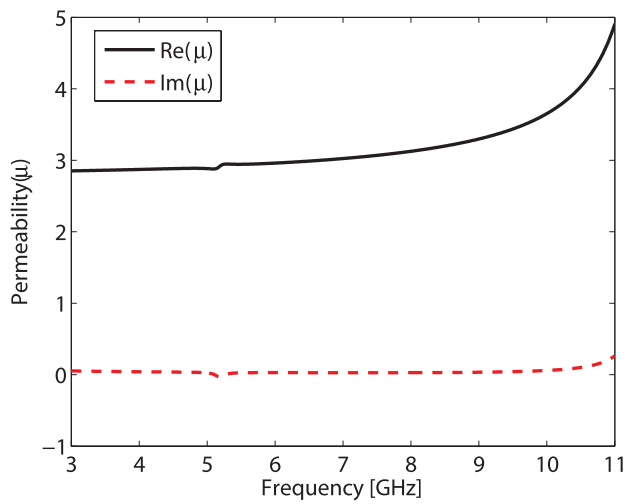
Figure 3.25: Retrieved parameters of the proposed unit cell for the first case: (a) Refractive index n, (b) Permittivity ε, (c) Permeability μ.

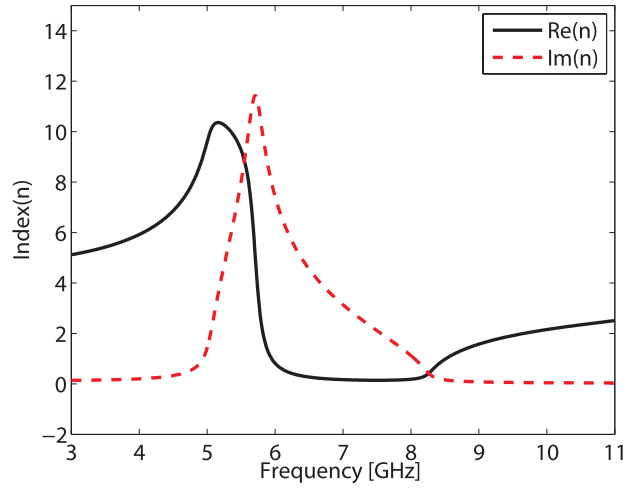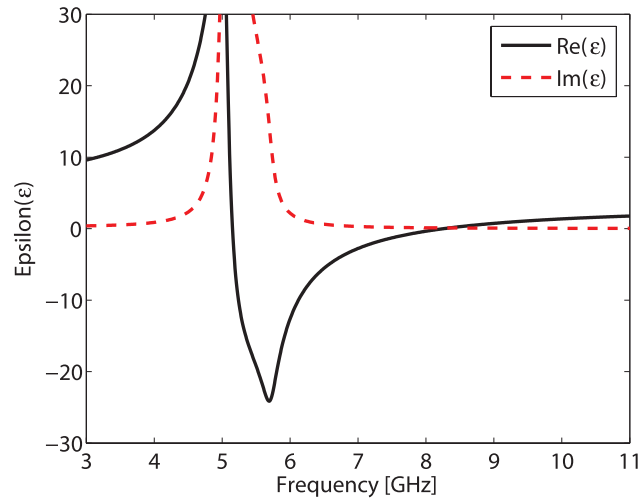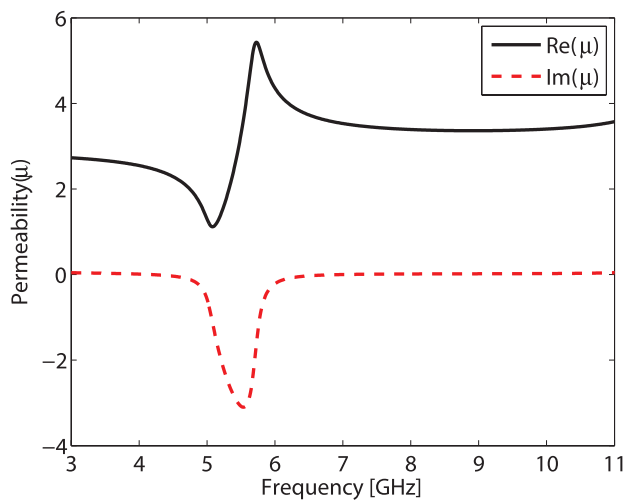Figure 3.26: Retrieved parameters of the proposed unit cell for the first case: (a) Refractive index n, (b) Permittivity ε, (c) Permeability μ.

b. Gain improvement of the designed antipodal Vivaldi antenna by using ZIM unit cells

Three configurations for the antipodal Vivaldi antenna (AVA) loaded with ZIM unit cells are shown in Figs. 3.27, 3.28 and 3.29. The proposed ZIM unit cells are placed and arranged in the upper layer of the printed circuit board. The configuration A has two columns of ZIM unit cells while the configuration B has three columns. The configuration C has a different arrangement to compare with the configurations A and B. The numbers $(1, 3, 5, 7, 9, 11, 15, 19)$ means the corresponding numbers of the ZIM unit cell on each columns.

To estimate which configuration has a better performance, we design the same length for these ones. The simulated return loss S_{11} and gain of the proposed configurations are presented in Figs. 3.30 and 3.31. Even the antipodal Vivaldi antenna adds the ZIM unit cells, the S_{11} is smaller than -10 dB in entire frequencies of UWB. It confirm that the proposed structures have a very good impedance matching. About gain, the configuration C has higher gain to compare with the configurations A and B. Therefore, the configuration C is chosen for improving the gain of the antipodal Vivaldi antenna.

The performance of the configuration C has been compared to the single antipodal Vivaldi antenna in Figs. 3.32 and 3.33. As can be observed that the maximum improved-gain band is correct with the stop-band of the ZIM unit cell (4.1 to 7.5 GHz) when wave propagating along x direction. At these frequencies, very few waves will propagate along x direction. Hence the energy will concentrate in y direction. In general, the gain of the designed antipodal Vivaldi antenna has been improved roughly 2 dB in a broadband from 3.0 to 7.5 GHz.

Figures 3.34 and 3.35 show the E field distribution at 5 GHz for the single antipodal Vivaldi antenna without and with ZIM unit cells, respectively. The antipodal Vivaldi antenna with ZIM unit cells has a strong and unniform field distribution while the single antipodal Vivaldi antenna has a weak and not uniform field distribution. Finally, we can conclude that by using ZIM unit cell to drive the wave propagation, the gain of the antipodal Vivaldi antenna can be enhanced.
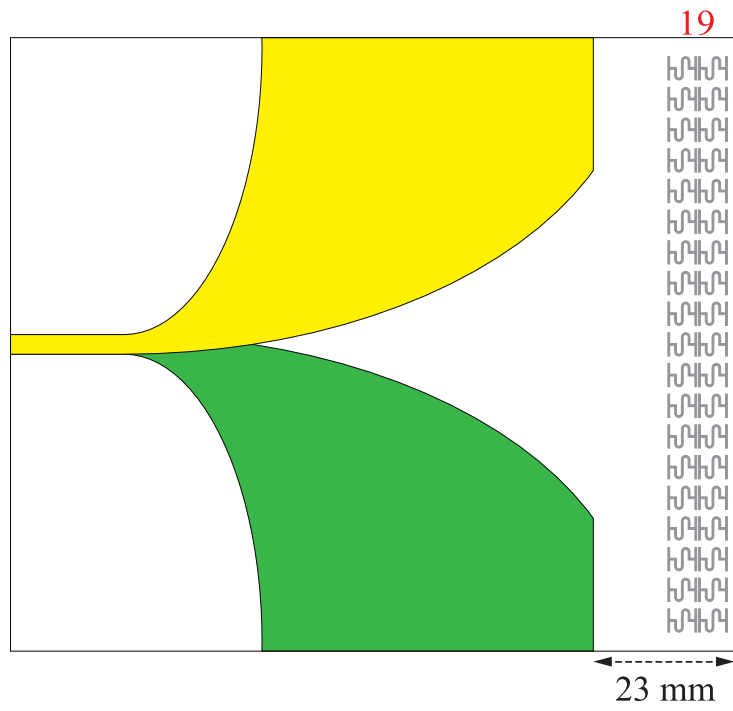
Figure 3.27: The configuration A
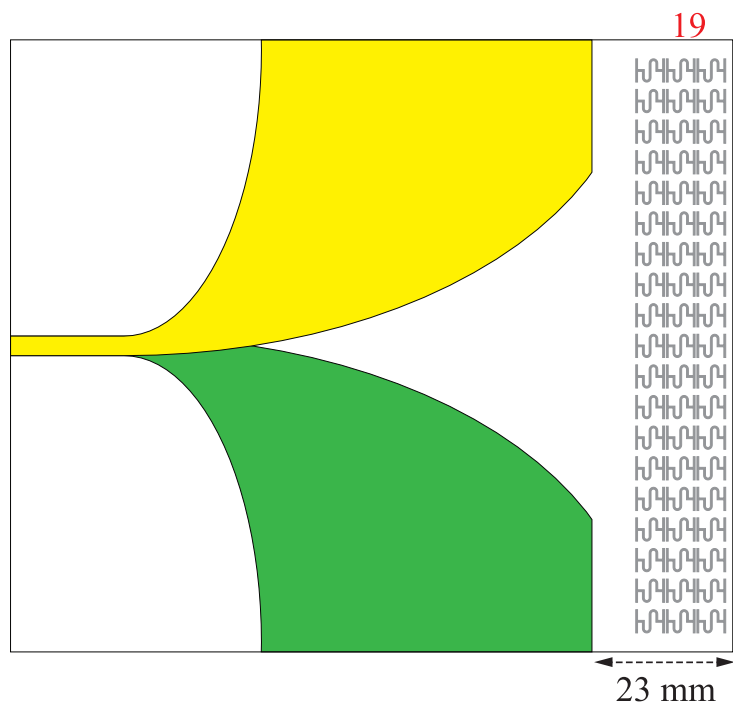
Figure 3.28: The configuration B
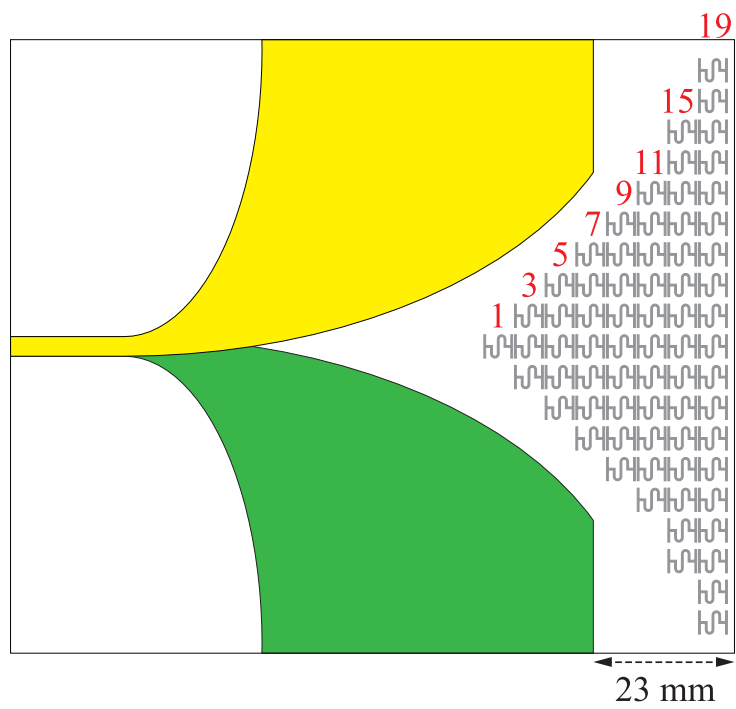
Figure 3.29: The configuration C
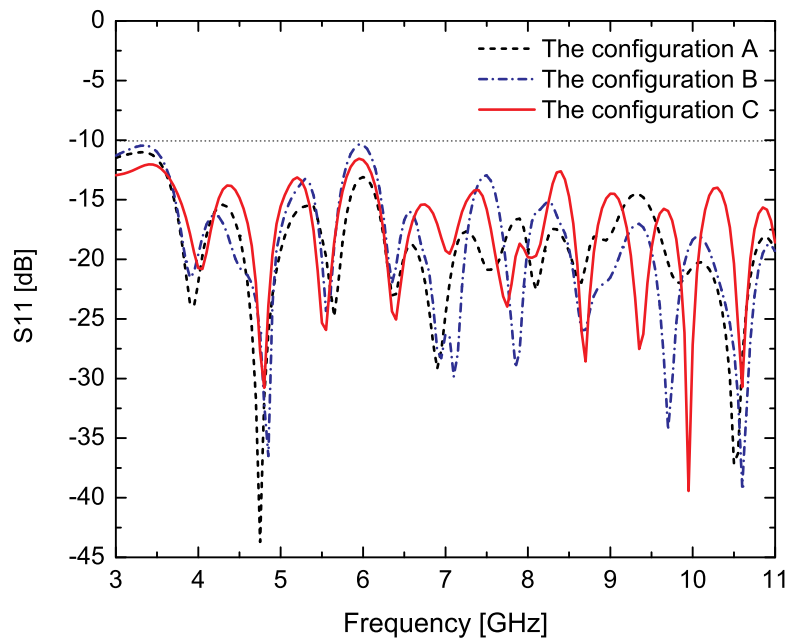
Figure 3.30: Simulated S11 for different configurations
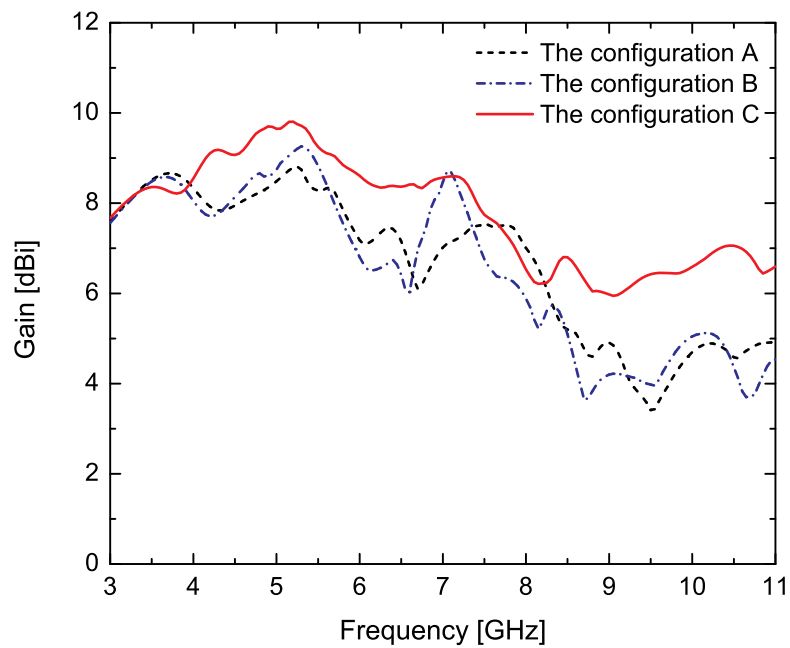
Figure 3.31: Simulated gain for different configurations
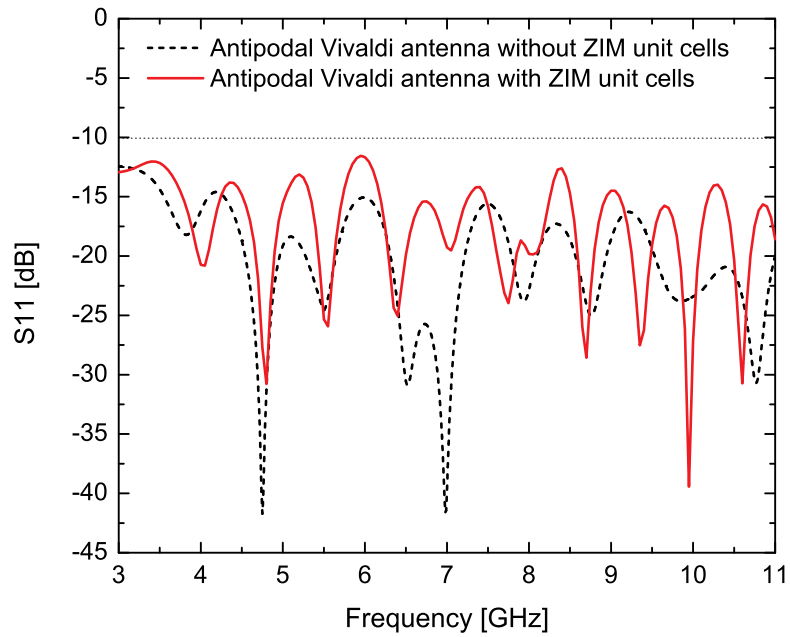
Figure 3.32: Simulated S-parameters for the antipodal Vivaldi antenna without and with ZIM unit cell (The configuration C)
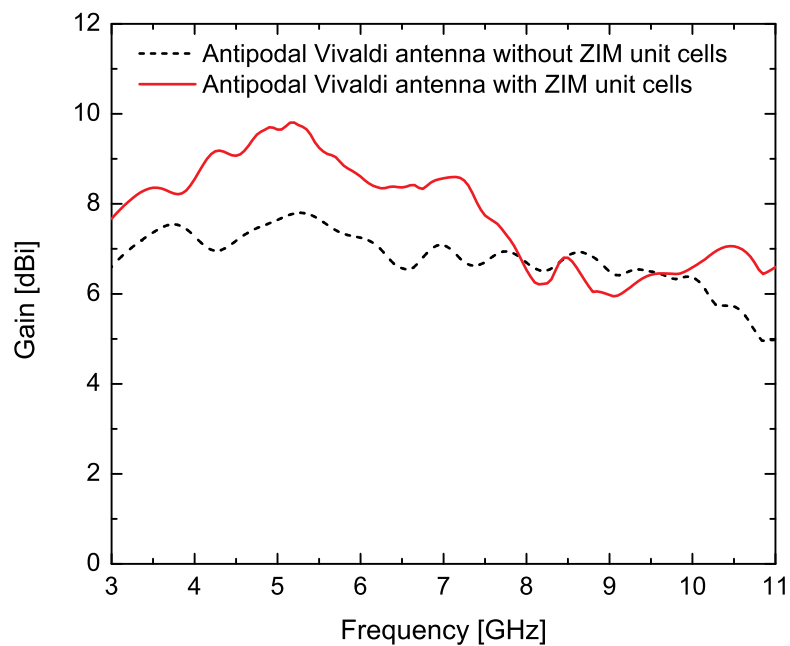
Figure 3.33: Simulated gain S-parameters for the antipodal Vivaldi antenna without and with ZIM unit cell (The configuration C)
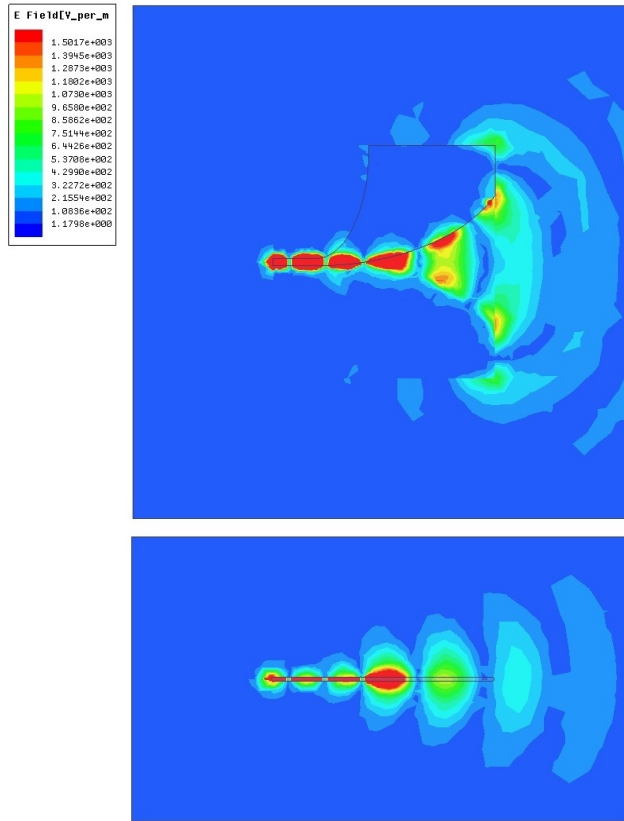
Figure 3.34: E field distribution at 5 GHz of the antipodal Vivaldi antenna.
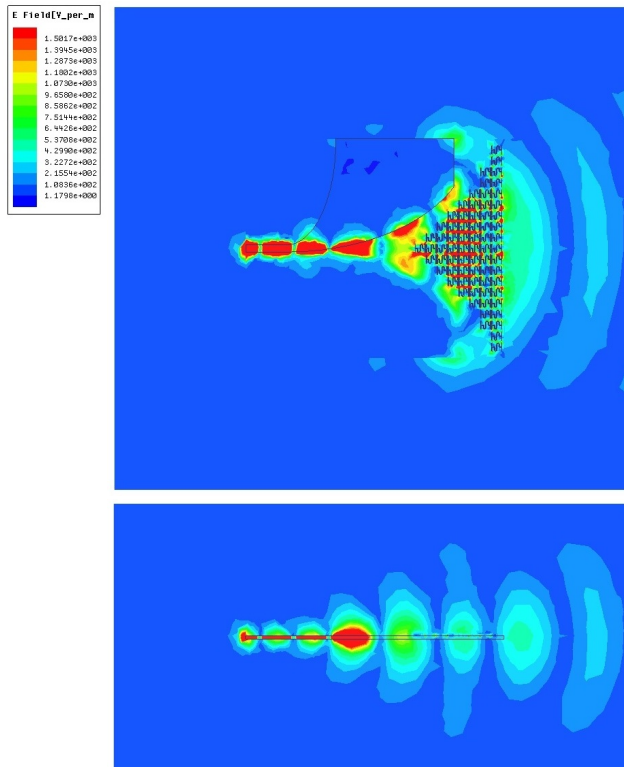
Figure 3.35: E field distribution at 5 GHz of the antipodal Vivaldi antenna wih ZIM unit cells (The configuration C).

97

Chapter 4

Conclusions and future works

4.1   Conclusions

This thesis has presented a new way for analysis and design of the E-CRLH TLs. All possible values of L–C elements to achieve the desired characteristics of the E-CRLH TLs are shown by using new closed-form solutions. Unlikely the previous methods, our method is helpful for various cases. The numerical results have demonstrated the usefulness of the method. Thus this study contributes to the theory and applications of the E-CRLH TLs, and its results can be applied to design dual-, tri- and quad-band RF and microwave devices. Then a compact quad-antenna has been designed from one E-CRLH TL unit cell. The resonant frequencies of the proposed antenna have been predicted from the theoretical L–C lumped elements and compared with simulated values. The proposed antenna shows advantages of small size, omnidirectional radiation characteristics, and easy fabrication of single copper layer on the low cost of FR4 substrate. Consequently, this antenna could be a candidate for multiband wireless communications.

Furthermore, an antipodal Vivaldi antenna has been designed for UWB applications. The antenna has been fabricated on the standard FR4 substrate, and various antenna properties have been measured. Then the measured results have been compared with those done by the HFSS, and good agreements show the validity and the quality of this antenna design method. The estimation formula of the low frequency end of the operational range is proposed and tested for various antennas designed by other authors. Our estimation formula has been found to give the best prediction among the other formulae. Lastly, the gain of the antipodal Vivaldi antenna has been improved in a broadband by using zero-index metamaterial (ZIM) unit cell to compare with the conventional methods.

4.2 Future works

Some innovative ideas were comprehensively explored in this research. Representative results from both simulations and experiments were presented. However additional work is needed to improve the current designs and to get more benefit from using metamaterials. The research work presented in this thesis can be further extended in following ways.

- Our current closed-form solutions for E-CRLH TL can be applied to design other devices such as filters, power dividers and directional couplers. In fact, the E-CRLH antenna can be redesigned in a better dielectric substrate than the low cost FR4 substrate to improve the current gain at 0.81 GHz.

- Knowledge from researched on CRLH, D-CRLH and E-CRLH TLs will be used to study a new metamaterial transmission line. And it is expected to become a useful transmission line for RF and microwave applications.

- The antipodal Vivaldi antenna loaded ZIM unit cell should be fabricated and measured to compare with the simulated results.

- A metamaterial slab with new resonant metamaterial unit cell will be developed for enhancing the efficiency of wireless power transfer systems. The concept of this metamaterial slab is to work as a microwave lens between the transmitting antenna and the receiving antenna of wireless power transfer systems. On the other hand, this is similar to improve the gain of the transmitting antenna.

List of Publications

Journal Papers

1. H. B. Chu, and H. Shirai, "A Compact Metamaterial Quad-band Antenna Based on Asymmetric E-CRLH unit cell," Progress In Electromagnetics Research C, Vol. 81, pp. 171–179, Feb. 2018.

2. H. B. Chu, and H. Shirai, "Analysis and Design of E-CRLH TL Characteristics with New Closed-Form Solutions," Progress In Electromagnetics Research C, Vol. 68, pp. 163–178, Oct. 2016.

3. H. B. Chu, H. Shirai, and D. N. Chien, "New Estimation Method for the Operational Low Frequency End of Antipodal Vivaldi Antennas," IEICE Transactions on Electronics, Vol. E99-C, No. 8, pp. 947–955, Aug. 2016.

International Conference Papers

1. H. B. Chu, and H. Shirai, "Design of Multiband Antennas Using Asymmetric E-CRLH TL Unit Cells," Proc. of the 2017 IEEE International Symposium on Antennas and Propagation, pp. 2531–2532, San Diego, USA, July 2017.

2. H. B. Chu, and H. Shirai, "Novel Closed-Form Solutions for Designing Extended-Composite Right/Left-Handed Transmission Lines," Proc. of International Conference on Electromagnetic in Advanced Applications, pp. 349–352, Cairns, Australia, Sept. 2016.

3. H. B. Chu, H. Shirai and D. N. Chien, "Effect of Curvature of Antipodal Structure on Vivaldi Antennas," Proc. of IEEE AP-S Symposium on Antennas and Propagation, pp. 2331–2332, Vancouver, Canada, July 2015.

4. H. B. Chu, H. Shirai and D. N. Chien, "Analysis and Design of Antipodal Vivaldi Antenna for UWB Applications," Proc. of International Conference on Communications and Electronics, pp. 391–394, Da Nang, Vietnam, July 2014.

5. H. B. Chu, H. Shirai and D. N. Chien, "High Efficiency Small Antenna for WLAN Application," Proc. of IEEE-APS Topical Conference on Antennas and Propagation in Wireless Communications, pp. 757–760, Turin, Italy, Sept. 2013.

6. H. B. Nguyen, H. B. Chu, and D. N. Chien, "All GPS bands Dielectric Resonator Antenna with Circular Polarization for GPS Applications," Proc. of International Conference on Advanced Technologies for Communications, pp. 65–68, Hanoi, Viet Nam, Oct. 2012.

Acknowledgment

Appendix A

A.1   Arc length of ellipses

From Fig. 3.7, the curve of the inner flare on the upper surface is given by Eq. (3.40), which may be written with a parameter t as

$$y_i = a_2\sqrt{1 - \cos^2 t} = a_2 \sin t = r_2 b_2 \sin t. \tag{A.1}$$

The intersection point A is given by setting $x = 0$ to get

$$y_A = a_2\sqrt{1 - \left(\frac{b_2 - w_f/2}{b_2}\right)^2} = a_2 \sin t_A, \tag{A.2}$$

where $t_A = \arccos\left\{1 - w_f/(2b_2)\right\}$. The flare end point $B(x_B, y_B = L_1)$ may be obtained from

$$x_B = b_2 \cos t_B - \left(b_2 - \frac{w_f}{2}\right), \tag{A.3}$$

where $t_B = \arcsin\left(L_1/a_2\right)$. Then the arc length L_- between points A and B becomes

$$L_- = a_2\left\{ \mathrm{E}\left(t_B, \sqrt{\frac{a_2^2 - b_2^2}{a_2^2}}\right) - \mathrm{E}\left(t_A, \sqrt{\frac{a_2^2 - b_2^2}{a_2^2}}\right) \right\},$$

where $\mathrm{E}(t, k)$ denotes the incomplete elliptic integral of the second kind [81]:

$$\mathrm{E}(t, k) = \int_0^t \sqrt{1 - k^2 \sin^2 t}\, dt. \tag{A.4}$$

A.2 Possible solutions for other cases

Two solutions for Eq. (2.104)

Solution 1:

$$
\begin{aligned}
C_1 &= \frac{B_0 + \sqrt{B_0^2 - 4A_0}}{2x_5 x_6 L_1}, \\
C_2 &= \left[\left(x_5 + x_6 - \frac{2x_5 x_6}{B_0 + \sqrt{B_0^2 - 4A_0}} - \frac{B_0 + \sqrt{B_0^2 - 4A_0}}{2} \right) L_1 \right]^{-1}, \\
L_2 &= \frac{2}{(B_0 + \sqrt{B_0^2 - 4A_0})C_2}, \\
C_3 &= \frac{2}{\left[(x_1 + x_2 + x_3 + x_4) - (x_5 + x_6 + x_7 + x_8) \right] L_1}, \\
L_3 &= \frac{B_0 - \sqrt{B_0^2 - 4A_0}}{2x_7 x_8 C_3}, \\
L_4 &= \left[\left(x_7 + x_8 - \frac{2x_7 x_8}{B_0 - \sqrt{B_0^2 - 4A_0}} - \frac{B_0 - \sqrt{B_0^2 - 4A_0}}{2} \right) C_3 \right]^{-1}, \\
C_4 &= \frac{2}{(B_0 - \sqrt{B_0^2 - 4A_0})L_4},
\end{aligned}
\tag{A.5}
$$

Solution 2:

$$
\begin{aligned}
C_1 &= \frac{B_0 - \sqrt{B_0^2 - 4A_0}}{2x_5 x_6 L_1}, \\
C_2 &= \left[\left(x_5 + x_6 - \frac{2x_5 x_6}{B_0 - \sqrt{B_0^2 - 4A_0}} - \frac{B_0 - \sqrt{B_0^2 - 4A_0}}{2} \right) L_1 \right]^{-1}, \\
L_2 &= \frac{2}{(B_0 - \sqrt{B_0^2 - 4A_0})C_2}, \\
C_3 &= \frac{2}{\left[(x_1 + x_2 + x_3 + x_4) - (x_5 + x_6 + x_7 + x_8) \right] L_1}, \\
L_3 &= \frac{B_0 + \sqrt{B_0^2 - 4A_0}}{2x_7 x_8 C_3}, \\
L_4 &= \left[\left(x_7 + x_8 - \frac{2x_7 x_8}{B_0 + \sqrt{B_0^2 - 4A_0}} - \frac{B_0 + \sqrt{B_0^2 - 4A_0}}{2} \right) C_3 \right]^{-1}, \\
C_4 &= \frac{2}{(B_0 + \sqrt{B_0^2 - 4A_0})L_4},
\end{aligned}
\tag{A.6}
$$

where A_0 and B_0 are calculated as follows:

$$
A_0 = \frac{D - [x_5 x_6 (x_7 + x_8) + x_7 x_8 (x_5 + x_6)]}{(x_1 + x_2 + x_3 + x_4) - (x_5 + x_6 + x_7 + x_8)},
\tag{A.7}
$$

$$
B_0 = \frac{E - [x_5 x_6 + x_7 x_8 + (x_5 + x_6)(x_7 + x_8)]}{(x_1 + x_2 + x_3 + x_4) - (x_5 + x_6 + x_7 + x_8)},
\tag{A.8}
$$

and other parameters D, E, x_i are the same as in Eqs. (2.113)$\sim$(2.115).

Two solutions for Eq. (2.105)

Solution 1:

$$C_1 = \frac{B_3 + \sqrt{B_3^2 - 4A_3}}{2x_5 x_8 L_1},$$

$$C_2 = \left[\left(x_5 + x_8 - \frac{2x_5 x_8}{B_3 + \sqrt{B_3^2 - 4A_3}} - \frac{B_3 + \sqrt{B_3^2 - 4A_3}}{2} \right) L_1 \right]^{-1},$$

$$L_2 = \frac{2}{(B_3 + \sqrt{B_3^2 - 4A_3})C_2},$$

$$C_3 = \frac{2}{[(x_1 + x_2 + x_3 + x_4) - (x_5 + x_6 + x_7 + x_8)] L_1}, \qquad \text{(A.9)}$$

$$L_3 = \frac{B_3 - \sqrt{B_3^2 - 4A_3}}{2x_6 x_7 C_3},$$

$$L_4 = \left[\left(x_6 + x_7 - \frac{2x_6 x_7}{B_3 - \sqrt{B_3^2 - 4A_3}} - \frac{B_3 - \sqrt{B_3^2 - 4A_3}}{2} \right) C_3 \right]^{-1},$$

$$C_4 = \frac{2}{(B_3 - \sqrt{B_3^2 - 4A_3})L_4},$$

Solution 2:

$$C_1 = \frac{B_3 - \sqrt{B_3^2 - 4A_3}}{2x_5 x_8 L_1},$$

$$C_2 = \left[\left(x_5 + x_8 - \frac{2x_5 x_8}{B_3 - \sqrt{B_3^2 - 4A_3}} - \frac{B_3 - \sqrt{B_3^2 - 4A_3}}{2} \right) L_1 \right]^{-1},$$

$$L_2 = \frac{2}{(B_3 - \sqrt{B_3^2 - 4A_3})C_2},$$

$$C_3 = \frac{2}{[(x_1 + x_2 + x_3 + x_4) - (x_5 + x_6 + x_7 + x_8)] L_1}, \qquad \text{(A.10)}$$

$$L_3 = \frac{B_3 + \sqrt{B_3^2 - 4A_3}}{2x_6 x_7 C_3},$$

$$L_4 = \left[\left(x_6 + x_7 - \frac{2x_6 x_7}{B_3 + \sqrt{B_3^2 - 4A_3}} - \frac{B_3 + \sqrt{B_3^2 - 4A_3}}{2} \right) C_3 \right]^{-1},$$

$$C_4 = \frac{2}{(B_3 + \sqrt{B_3^2 - 4A_3})L_4},$$

where A_3 and B_3 are calculated as follows:

$$A_3 = \frac{D - [x_5 x_8 (x_6 + x_7) + x_6 x_7 (x_5 + x_8)]}{(x_1 + x_2 + x_3 + x_4) - (x_5 + x_6 + x_7 + x_8)}, \qquad \text{(A.11)}$$

$$B_3 = \frac{E - [x_5 x_8 + x_6 x_7 + (x_5 + x_8)(x_6 + x_7)]}{(x_1 + x_2 + x_3 + x_4) - (x_5 + x_6 + x_7 + x_8)}, \qquad \text{(A.12)}$$

and other parameters D, E, x_i are the same as in Eqs. (2.113)~(2.115).

Two solutions for Eq. (2.106)

Solution 1:

$$
\begin{aligned}
C_1 &= \frac{B_4 + \sqrt{B_4^2 - 4A_4}}{2x_6 x_8 L_1}, \\
C_2 &= \left[\left(x_6 + x_8 - \frac{2x_6 x_8}{B_4 + \sqrt{B_4^2 - 4A_4}} - \frac{B_4 + \sqrt{B_4^2 - 4A_4}}{2} \right) L_1 \right]^{-1}, \\
L_2 &= \frac{2}{(B_4 + \sqrt{B_4^2 - 4A_4})C_2}, \\
C_3 &= \frac{2}{[(x_1 + x_2 + x_3 + x_4) - (x_5 + x_6 + x_7 + x_8)] L_1}, \qquad\qquad \text{(A.13)}\\
L_3 &= \frac{B_4 - \sqrt{B_4^2 - 4A_4}}{2x_5 x_7 C_3}, \\
L_4 &= \left[\left(x_5 + x_7 - \frac{2x_5 x_7}{B_4 - \sqrt{B_4^2 - 4A_4}} - \frac{B_4 - \sqrt{B_4^2 - 4A_4}}{2} \right) C_3 \right]^{-1}, \\
C_4 &= \frac{2}{(B_4 - \sqrt{B_4^2 - 4A_4})L_4},
\end{aligned}
$$

Solution 2:

$$
\begin{aligned}
C_1 &= \frac{B_4 - \sqrt{B_4^2 - 4A_4}}{2x_6 x_8 L_1}, \\
C_2 &= \left[\left(x_6 + x_8 - \frac{2x_6 x_8}{B_4 - \sqrt{B_4^2 - 4A_4}} - \frac{B_4 - \sqrt{B_4^2 - 4A_4}}{2} \right) L_1 \right]^{-1}, \\
L_2 &= \frac{2}{(B_4 - \sqrt{B_4^2 - 4A_4})C_2}, \\
C_3 &= \frac{2}{[(x_1 + x_2 + x_3 + x_4) - (x_5 + x_6 + x_7 + x_8)] L_1}, \qquad\qquad \text{(A.14)}\\
L_3 &= \frac{B_4 + \sqrt{B_4^2 - 4A_4}}{2x_5 x_7 C_3}, \\
L_4 &= \left[\left(x_5 + x_7 - \frac{2x_5 x_7}{B_4 + \sqrt{B_4^2 - 4A_4}} - \frac{B_4 + \sqrt{B_4^2 - 4A_4}}{2} \right) C_3 \right]^{-1}, \\
C_4 &= \frac{2}{(B_4 + \sqrt{B_4^2 - 4A_4})L_4},
\end{aligned}
$$

where A_4 and B_4 are calculated as follows:

$$
A_4 = \frac{D - [x_6 x_8 (x_5 + x_7) + x_6 x_8 (x_5 + x_7)]}{(x_1 + x_2 + x_3 + x_4) - (x_5 + x_6 + x_7 + x_8)}, \qquad\qquad \text{(A.15)}
$$

$$
B_4 = \frac{E - [x_6 x_8 + x_5 x_7 + (x_6 + x_8)(x_5 + x_7)]}{(x_1 + x_2 + x_3 + x_4) - (x_5 + x_6 + x_7 + x_8)}, \qquad\qquad \text{(A.16)}
$$

and other parameters D, E, x_i are the same as in Eqs. (2.113)∼(2.115).

Two solutions for Eq. (2.107)

Solution 1:

$$
\begin{aligned}
C_1 &= \frac{B_5 + \sqrt{B_5^2 - 4A_5}}{2x_7 x_8 L_1}, \\
C_2 &= \left[\left(x_7 + x_8 - \frac{2x_7 x_8}{B_5 + \sqrt{B_5^2 - 4A_5}} - \frac{B_5 + \sqrt{B_5^2 - 4A_5}}{2} \right) L_1 \right]^{-1}, \\
L_2 &= \frac{2}{(B_5 + \sqrt{B_5^2 - 4A_5})C_2}, \\
C_3 &= \frac{2}{[(x_1 + x_2 + x_3 + x_4) - (x_5 + x_6 + x_7 + x_8)] L_1}, \\
L_3 &= \frac{B_5 - \sqrt{B_5^2 - 4A_5}}{2x_5 x_6 C_3}, \\
L_4 &= \left[\left(x_5 + x_6 - \frac{2x_5 x_6}{B_5 - \sqrt{B_5^2 - 4A_5}} - \frac{B_5 - \sqrt{B_5^2 - 4A_5}}{2} \right) C_3 \right]^{-1}, \\
C_4 &= \frac{2}{(B_5 - \sqrt{B_5^2 - 4A_5})L_4},
\end{aligned}
\tag{A.17}
$$

Solution 2:

$$
\begin{aligned}
C_1 &= \frac{B_5 - \sqrt{B_5^2 - 4A_5}}{2x_7 x_8 L_1}, \\
C_2 &= \left[\left(x_7 + x_8 - \frac{2x_7 x_8}{B_5 - \sqrt{B_5^2 - 4A_5}} - \frac{B_5 - \sqrt{B_5^2 - 4A_5}}{2} \right) L_1 \right]^{-1}, \\
L_2 &= \frac{2}{(B_5 - \sqrt{B_5^2 - 4A_5})C_2}, \\
C_3 &= \frac{2}{[(x_1 + x_2 + x_3 + x_4) - (x_5 + x_6 + x_7 + x_8)] L_1}, \\
L_3 &= \frac{B_5 + \sqrt{B_5^2 - 4A_5}}{2x_5 x_6 C_3}, \\
L_4 &= \left[\left(x_5 + x_6 - \frac{2x_5 x_6}{B_5 + \sqrt{B_5^2 - 4A_5}} - \frac{B_5 + \sqrt{B_5^2 - 4A_5}}{2} \right) C_3 \right]^{-1}, \\
C_4 &= \frac{2}{(B_5 + \sqrt{B_5^2 - 4A_5})L_4},
\end{aligned}
\tag{A.18}
$$

where A_5 and B_5 are calculated as follows:

$$
A_5 = \frac{D - [x_7 x_8 (x_5 + x_6) + x_7 x_8 (x_5 + x_6)]}{(x_1 + x_2 + x_3 + x_4) - (x_5 + x_6 + x_7 + x_8)},
\tag{A.19}
$$

$$
B_5 = \frac{E - [x_7 x_8 + x_5 x_6 + (x_7 + x_8)(x_5 + x_6)]}{(x_1 + x_2 + x_3 + x_4) - (x_5 + x_6 + x_7 + x_8)},
\tag{A.20}
$$

and other parameters D, E, x_i are the same as in Eqs. (2.113)~(2.115).

Two solutions for Eq. (2.108)

Solution 1:

$$
C_1 = \frac{B_6 + \sqrt{B_6^2 - 4A_6}}{2x_6 x_7 L_1},
$$

$$
C_2 = \left[\left(x_6 + x_7 - \frac{2x_6 x_7}{B_6 + \sqrt{B_6^2 - 4A_6}} - \frac{B_6 + \sqrt{B_6^2 - 4A_6}}{2} \right) L_1 \right]^{-1},
$$

$$
L_2 = \frac{2}{(B_6 + \sqrt{B_6^2 - 4A_6})C_2},
$$

$$
C_3 = \frac{2}{[(x_1 + x_2 + x_3 + x_4) - (x_5 + x_6 + x_7 + x_8)] L_1}, \tag{A.21}
$$

$$
L_3 = \frac{B_6 - \sqrt{B_6^2 - 4A_6}}{2x_5 x_8 C_3},
$$

$$
L_4 = \left[\left(x_5 + x_8 - \frac{2x_5 x_8}{B_6 - \sqrt{B_6^2 - 4A_6}} - \frac{B_6 - \sqrt{B_6^2 - 4A_6}}{2} \right) C_3 \right]^{-1},
$$

$$
C_4 = \frac{2}{(B_6 - \sqrt{B_6^2 - 4A_6})L_4},
$$

Solution 2:

$$
C_1 = \frac{B_6 - \sqrt{B_6^2 - 4A_6}}{2x_6 x_7 L_1},
$$

$$
C_2 = \left[\left(x_6 + x_7 - \frac{2x_6 x_7}{B_6 - \sqrt{B_6^2 - 4A_6}} - \frac{B_6 - \sqrt{B_6^2 - 4A_6}}{2} \right) L_1 \right]^{-1},
$$

$$
L_2 = \frac{2}{(B_6 - \sqrt{B_6^2 - 4A_6})C_2},
$$

$$
C_3 = \frac{2}{[(x_1 + x_2 + x_3 + x_4) - (x_5 + x_6 + x_7 + x_8)] L_1}, \tag{A.22}
$$

$$
L_3 = \frac{B_6 + \sqrt{B_6^2 - 4A_6}}{2x_5 x_8 C_3},
$$

$$
L_4 = \left[\left(x_5 + x_8 - \frac{2x_5 x_8}{B_6 + \sqrt{B_6^2 - 4A_6}} - \frac{B_6 + \sqrt{B_6^2 - 4A_6}}{2} \right) C_3 \right]^{-1},
$$

$$
C_4 = \frac{2}{(B_6 + \sqrt{B_6^2 - 4A_6})L_4},
$$

where A_6 and B_6 are calculated as follows:

$$
A_6 = \frac{D - [x_6 x_7 (x_5 + x_8) + x_5 x_8 (x_6 + x_7)]}{(x_1 + x_2 + x_3 + x_4) - (x_5 + x_6 + x_7 + x_8)}, \tag{A.23}
$$

$$
B_6 = \frac{E - [x_6 x_7 + x_5 x_8 + (x_6 + x_7)(x_5 + x_8)]}{(x_1 + x_2 + x_3 + x_4) - (x_5 + x_6 + x_7 + x_8)}, \tag{A.24}
$$

and other parameters D, E, x_i are the same as in Eqs. (2.113)∼(2.115).

References

[1] V. G. Veselago, "The electrodynamics of substances with simultaneously negative values of ε and μ," *Soviet Physics Uspekhi*, vol. 10, pp. 509−514, Feb. 1968.

[2] J. B. Pendry, A. J. Holden, D. J. Robbins, and W. J. Stewart, "Low frequency plasmons in thin-wire structures," J. Phys. Condens. Matter, vol. 10, pp. 4785–4809, 1998.

[3] J. B. Pendry, A. J. Holden, D. J. Robbins, and W. J. Stewart, "Magnetism from conductors and enhanced nonlinear phenomena," *IEEE Trans. Microwave Theory Tech.*, vol. MTT-47, pp. 2075−2084, Nov. 1999.

[4] R. A. Shelby, D. R. Smith, and S. Schultz, "Experimental verification of a negative index of refraction," *Science*, vol. 292, pp. 77−79, Apr. 2001.

[5] A. K. Iyer and G. V. Eleftheriades, "Negative refractive index metamaterials supporting 2-D waves," *Proc. of IEEE-MTT International Microwave Symposium Digest*, vol. 2, pp. 412–415, June 2002.

[6] A. A. Oliner, "A periodic-structure negative-refractive-index medium without resonant elements," *Proc. of URSI Digest, IEEE-AP-S USNC/URSI National Radio Science Meeting*, pp. 41, June 2002.

[7] C. Caloz and T. Itoh, "Application of the transmission line theory of left-handed (LH) materials to the realization of a microstrip LH transmission line," *Proc. of IEEE-AP-S USNC/URSI National Radio Science Meeting*, vol. 2, pp. 412–415, June 2002.

[8] C. Caloz, and T. Itoh, *Electromagnetic Metamaterials Transmission Line Theory and Microwave Applications*, John Wiley & Sons, 2006.

[9] C. Caloz, "Dual composite right/left-handed (D-CRLH) transmission line metamaterial," *IEEE Microwave and Wireless Components Letters*, vol. 16, no. 11, 585–587, Nov. 2006.

[10] A. Rennings, S. Otto, J. Mosig, C. Caloz and I. Wolff, "Extended composite right/left-handed (E-CRLH) metamaterial and its application as quadband quarter-wavelength transmission line," *Proc. of Asia-Pacific Microwave Conference*, pp. 1405–1408, Dec. 2006.

[11] G. V. Eleftheriades, "A generalized negative-refractive-index transmission line (NRL-TL) metamaterial for dual-band and quad-band applications," *IEEE Microwave and Wireless Component Letters*, vol. 17, no. 6, 415–417, June 2007.

[12] J. Y. Rhee, Y. J. Yoo, K. W. Kim, Y. J. Kim and Y. P. Lee, "Metamaterial-based perfect absorbers," *Journal of Electromagnetic Waves and Applications*, vol. 28, no. 13, pp. 1541-1580, Aug. 2014.

[13] A. K. Iyer, and G. V. Eleftheriades, "Free-space imaging beyond the diffraction limit using a Veselago-Pendry transmission-line metamaterial superlens," *IEEE Transactions on Antennas and Propagation*, vol. 57, no.6, June 2009.

[14] B. I. Wu, W. Wang, J. Pacheco, X. Chen, T. Grzegorczyk and J. A. Kong, "A study of using metamaterials as antenna substrate to enhance gain" *Progress In Electromagnetics Research*, pp. 295–328, 2005.

[15] B. Wang, W. Yerazunis, K. H. Teo, "Wireless power transfer with metamaterials," *Mitsubishi Electric Research Laboratories*, April 2011.

[16] Y. Urzhumov, and D. R. Smith, "Metamaterial-enhanced coupling between magnetic dipoles for efficient wireless power transfer," *Physical Review B*, vol. 83, no.20, May 2011.

[17] G. Lipworth, J. Ensworth, K.l Seetharam1, D. Huang, J. S. Lee, P. Schmalenberg, T. Nomura, M. S. Reynolds, D. R. Smith, and Y. Urzhumov, "Magnetic metamaterial superlens for increased range wireless power transfer," *Scientific Reports*, Jan. 2014.

[18] D. M. Pozar, *Microwave Engineering*, John Wiley & Sons, 2012.

[19] G. V. Eleftheriades, "Design of generalised negative-refractive-index transmission lines for quad-band applications," *IET Microwaves, Antennas and Propagation*, vol. 4, no. 8, pp. 977–981, Aug. 2010.

[20] M. Fozi, S. Nikmehr, M. V. Ghurt-Tappeh and M. Bemani, "Design of dual- and quad-band E-CRLH-TLs with arbitrary phase characteristics," *Progress In Electromagnetics Research M*, vol. 35, pp. 141–149, Mar. 2014.

[21] L. Peng, and C. I. Ruan, "Design, analysis and implementation of novel metamaterial transmission line with dual composite right/left-handed and conventional composite

right/left-handed properties," *IET Microwaves, Antennas and Propagation*, vol. 6, no. 15, pp. 1687–1695, Oct. 2012.

[22] J. Anguera, A. Andujar, M.C. Huynh, C. Orlenius, C. Picher, and C. Puente, "Advances in Antenna Technology for Wireless Handheld Devices," *International Journal on Antennas and Propagation*, volume 2013, Article ID 838364.

[23] C. P. Lin, C. H. Chang, and C. F. Jou, "Compact quad-band monopole antenna," *Microwave and Optical Technology Letters*, vol. 53, no. 6, pp. 1272–1276, June 2011.

[24] X. Sun, G. Zeng, H. C. Yang, Y. Li, X. J. Liao, and L. Wang, "Design of an edge-fed quad-band slot antenna for GPS/WiMAX/WLAN applications," *Progress In Electromagnetics Research Letters*, vol. 28, pp. 111–120, Dec. 2011.

[25] Y. F. Cao, S. W. Cheung and T. I. Yuk , "A Multiband Slot Antenna for GPS/WiMAX/WLAN Systems," *IEEE Transaction on Antennas and Propagation*, vol. 63, no. 3, pp. 952–958, March 2015.

[26] L. Xiong, P. Gao, and P. J. Tang, "Quad-band rectangular wide-slot antenna for GPS/ WiMAX/WLAN applications," *Progress In Electromagnetics Research C*, vol. 30, pp. 201–2011, June 2012.

[27] X. Sun, G. Zeng, H. C. Yang, and Y. Li, "A compact quad-band CPW-Fed slot antenna for M-WiMAX/WLAN applications," *IEEE Antennas and Wireless Propagation Letters*, vol. 11, pp. 395–398, April 2012.

[28] R. S. Aziz, M. A. S. Alkanhal, and A. F. A. Sheta, "Multiband fractal-like antennas," *Progress In Electromagnetics Research B*, vol. 29, pp. 339–354, April 2011.

[29] H. Liu, P. Wen, S. Zhu, B. Ren, X. Guan and H. Yu, "Quad-band CPW-fed monopole antenna based on flexible pentangle-loop radiator," *IEEE Antennas and Wireless Propagation Letters*, vol. 14, pp. 1373–1376, Feb. 2015.

[30] R. Azaro, F. Viani, L. Lizzi, E. Zeni and A. Massa, "A monopolar quad-band antenna based on a Hilbert self-affine prefractal geometry," *IEEE Antennas and Wireless Propagation Letters*, vol. 8, pp. 177–180, April 2009.

[31] S. Risco, J. Anguera, A. Andujar, A. Perez, and C. Puente, "Coupled Monopole Antenna Design for Multiband Handset Devices," *Microwave and Optical Technology Letters*, vol.52, no. 10, pp. 359–364, Feb. 2010.

[32] H. Xu, H. Wang, S. Gao, H. Zhou, Y. Huang, Q. Xu, and Y. Cheng, "A Compact and Low-Profile Loop Antenna With Six Resonant Modes for LTE Smartphone," *IEEE Transactions on Antennas and Propagation*, vol. 64, no. 9, pp. 3743–3751, Sept. 2016.

[33] J. Anguera, C. Picher, A. Bujalance, and A. Andujar, "Ground Plane Booster Antenna Technology for Smartphones and Tablets," *Microwave and Optical Technology Letters*, vol.58, no. 6, pp.1289–1294, June 2016.

[34] W. H. Lee, A. Gummalla, and M. Achour, "Small antennas based on CRLH structures: concept, design, and applications," *IEEE Antenna and Propagation Magazine*, vol. 53, no. 2, pp. 11–25, April 2011.

[35] L. Li, J. Zhen, F. Huo, and W. Han, "A novel compact multiband antenna employing dual-band CRLH-TL for smart mobile phone application," *IEEE Antennas and Wireless Propagation Letters*, vol. 12, pp. 1688–1691, Dec. 2013.

[36] A. A. Ibrahim, A. M. E. Sfwat, and H. El-Hennawy, "Triple-band microstrip-fed monopole antenna loaded with CRLH unit cell," *IEEE Antennas and Wireless Propagation Letter*, vol. 10, pp. 1547–1550, Dec. 2011.

[37] Y. H. Ryu, J. H. Park, J. H. Lee, and H. S. Tae,"Multiband antenna using +1, −1, and 0 resonant mode of DGS dual composite right left handed transmission line," *Microwave and Optical Technology Letters*, vol. 51, no. 10, pp. 2485–2488, Oct. 2009.

[38] H. N. Quang, and H. Shirai, "A compact tri-band metamaterial antenna for WLAN and WiMAX applications," *Proc. of International Conference on Electromagnetics in Advanced Applications*, pp. 133–136, Sept. 2015.

[39] C. G. M. Ryan, and G. V. Eleftheriades, "A dual-band leaky-wave antenna based on generalized negative-refractive-index transmission-lines," *Proc. of IEEE International Symposium on Antennas and Propagation*, pp. 1–4, July 2010.

[40] M. Duran-Sindreu, J. Choi, J. Bonache, F. Martin, and T. Itoh, "Dual-band leaky wave antenna with filtering capability based on extended-composite right/left-handed transmission lines," *Proc. of IEEE MTT-S International Microwave Symposium Digest*, June 2013.

[41] M. A. Abdalla, and M. A. Fouad, "CPW dual-band antenna based on asymmetric generalized metamaterial π NRI transmission line for ultra compact applications," *Progress In Electromagnetics Research C*, vol. 62, pp. 99–107, Feb. 2016.

[42] X. Gao, T. J. Jackson, and P. Gardner, "Multiband open-ended resonant antenna based on one ECRLH unit cell structure," *IEEE Antennas and Wireless Propagation Letters*, vol. 16, pp. 1273–1276, May 2017.

[43] M. R. Booket, M. Veysi, Z. Atlasbaf and A. Jafargholi, "Ungrounded composite right-/left-handed metamaterials: design, synthesis and applications," *IET Microwaves, Antennas and Propagation*, vol. 6, no. 11, pp. 1259–1268, May 2012.

[44] P. L. Shu, and Q. I. Feng, "Design of a compact quad-band hybrid antenna for COMPASS/ WiMAX/WLAN applications," *Progress In Electromagnetics Research*, vol. 138, pp. 585–598, April 2013.

[45] X. Chen, T. M. Grzegorczyk, B. I. Wu, J. Pacheco and J. A. Kong, "Robust method to retrieve the constitutive effective parameters of metamaterials," *Physical Review E* 70, 016608, July 2004.

[46] D. R. Smith, D. C. Vier, Th. Koschny, and C. M. Soukoulis, "Electromagnetic parameter retrieval from inhomogeneous metamaterials," *Physical Review E* 71, 036617, March 2005.

[47] Federal Communication Commission FCC 02–48, 2002.

[48] P. J. Gibson, "The Vivaldi aerial," *Proc. 9th European Microwave Conference*, pp. 101–105, Sept. 1979.

[49] E. Gazit, "Improved design of Vivaldi antenna," *IEE Proc. Microwaves, Antennas and Propagation*, vol. 135, no. 2, pp. 89–92, April 1988.

[50] J. D. S. Langley, P. S. Hall and P. Newham, "Novel ultra wide-bandwidth Vivaldi antenna with low cross polarization," *Electronic Letters*, vol. 29, no.23, pp. 2004–2005, Nov. 1993.

[51] J. D. S. Langley, P. S. Hall and P. Newham, "Balanced antipodal Vivaldi antenna for wide bandwidth phased arrays," *IEE Proc. Microwaves, Antennas and Propagation*, vol. 143, no. 2, April 1996.

[52] S. G. Kim and K. Chang, "Ultra wideband exponentially-tapered antipodal Vivaldi antennas," *Proc. IEEE International Symposium on Antennas and Propagation Society*, pp. 2273–2276, June 2004.

[53] F. Guangyou, "New design of the antipodal Vivaldi antenna for a GPR system," *Microwave and Optical Technology Letters*, vol. 44, no.2, pp. 136–139, Jan. 2005.

[54] X. Qing, Z. N. Chen and M. Y. W. Chia, "Dual elliptically tapered antipodal slot antenna loaded by curved terminations for ultra wideband applications," *Radio Science*, vol. 41, RS6009, 2006.

[55] H. B. Chu, H. Shirai and C. D. Ngoc, "Analysis and design of antipodal Vivaldi antenna for UWB applications," *Proc. of 2014 IEEE International Conference on Communications and Electronics*, pp. 391–394, Aug. 2014.

[56] A. Dastranj, "Wideband antipodal Vivaldi antenna with enhanced radiation parameters," *IET Microwaves, Antennas and Propagation*, vol. 9, no. 15, pp. 1755–1760, July 2015.

[57] H. Sato, Y. Takagi and K. Sawaya, "High gain antipodal Fermi antenna with low cross polarization," *IEICE Trans. Commun.*, vol. E94-B, no. 8, pp. 2292–2297, Aug. 2011.

[58] J. Bai, S. Shi and D. W. Prather, "Modified compact antipodal Vivaldi antenna for 4-50 GHz UWB application," *IEEE Trans. Microwave Theory and Tech.*, vol. 59, no. 4, pp. 1051–1057, April 2011.

[59] P. Wang, H. Zhang, G. Wen and Y. Sun, "Design of modified 6-18 GHz balanced antipodal Vivaldi antenna," *Progress In Electromagnetics Research C*, vol. 25, pp. 271–285, 2012.

[60] G. Teni, N. Zhang, J. Qiu and P. Zhang, "Research on a novel miniaturized antipodal Vivaldi antenna with improved radiation," *IEEE Antennas and Wireless Propagation Letters*, vol. 12, pp. 417–420, March 2013.

[61] De Oliveira AM, Perotoni MB, Kofuji ST, Justo JF., "A palm tree antipodal Vivaldi antenna with exponential slot edge for improved radiation pattern," *IEEE Antennas Wireless Propag. Lett.*, pp. 1334–1337, 2015.

[62] Herzi R, Zairi H, Gharsallah A. "Reconfigurable Vivaldi antenna with improved gain for UWB application," *Microw Opt Techn. Lett.*, pp. 490–494, 2016.

[63] A. Dastranj, "Wideband antipodal Vivaldi antenna with enhanced radiation parameters," *IET Microwave, Antennas and Propagation*, pp. 1755–1760, 2015.

[64] Bourqui J, Okoniewski M, Fear EC., "Balanced antipodal Vivaldi antenna with dielectric director for near-field microwave imaging," *IEEE Trans. Antenna Propag.*, pp. 2318–2326, 2010.

[65] Kota K, Shafai L., "Gain and radiation pattern enhancement of balanced antipodal Vivaldi antenna," *Electron Lett.*, pp. 303–304, 2011.

[66] Molaei A, Kaboli M, Mirtaheri SA, Abrishamian MS., "Dielectric lens balanced antipodal Vivaldi antenna with low crosspolarisation for ultra-wideband applications," *IET Microwave Antennas Propag.*, pp. 1137–1142, 2014

[67] I. T. Nassar and T. M. Weller, "A novel method for improving antipodal Vivaldi antenna performance," *IEEE Transactions on Antennas and Propagation*, pp. 3321–3324, 2015

[68] Akhter ZABN, Akhtar MJ., "Hemisphere lens-loaded Vivaldi antenna for time domain microwave imaging of concealed objects," *J. Electromagn. Waves Appl.*, pp. 1183–1197, 2016.

[69] M. C. Greenberg, K. L. Virga and C. L. Hammond, "Performance characteristics of the dual exponentially tapered slot antenna (DETSA) for wireless communications application," *IEEE Trans. Vehicular Tech.*, vol. 52, no. 2, pp. 305–312, March 2003.

[70] S. Wang, X. D. Chen and C. G. Parini, "Analysis of ultra wideband antipodal Vivaldi antenna design," *Proc. of Loughborough Antennas and Propagation Conference*, pp. 129–132, April 2007.

[71] P. Fei, Y. C. Jiao, W. Hu and F. S. Zhang, "A miniaturized antipodal Vivaldi antenna with improved radiation characteristics," *IEEE Antennas and Wireless Propagation Letters*, vol. 10, pp. 127–130, March 2011.

[72] A. M. De Oliveira, M. B. Perotoni, S. T. Kofuji and J. F. Justo, "A palm tree antipodal Vivaldi antenna with exponential slot edge for improved radiation pattern," *IEEE Antennas and Wireless Propagation Letters*, vol. 14, pp. 1334–1337, Feb. 2015.

[73] F. Zhu and S. Gao, "Compact elliptically tapered slot antenna with non-uniform corrugations for ultra-wideband application," *Radio Engineering*, vol. 22, no. 1, pp. 276–280, April 2013.

[74] B. J. Mohammed, A. M. Abbosh and P. Sharpe, "Planar array of corrugated tapered slot antennas for ultra wideband biomedical microwave imaging system," International Journal of RF and Microwave Computer-Aided Engineering, vol. 23, no. 1, pp. 59–66, May 2012.

[75] A. M. Abbosh, H. K. Kan and M. E. Bialkowski, "Compact ultra-wideband planar tapered slot antenna for use in a microwave imaging system," *Microwave and Optical Technology Letters*, vol. 48, no. 11, pp. 2212–2216, Nov. 2006

[76] G. Fang and M. Sato, "Optimization of Vivaldi Antenna for Demining by GPR," *Proc. of International Symposium on Antennas and Propagation*, pp. 263–266, Nov. 2002.

[77] T. H. Chio and D. H. Schaubert, "Parameter study and design of wide-band wide scan dual-polarized tapered slot antenna arrays," *IEEE Trans. Antennas and Propag.*, vol. 48, no. 6, pp. 879–886, June 2000.

[78] E. de Lera Acedo, E. Garcia, V. Gonzalez-Posadas, J. L. Vazquez-Roy, R. Maaskant and D. Segovia, "Study and design of a differentially fed tapered slot antenna array," *IEEE Trans. Antennas and Propag.*, vol. 58, no. 1, pp. 68–78, Jan. 2010.

[79] K. Nakada and H. Arai, "Tapered slot antenna excited by proximity coupled dipole antenna," *Proc. of Asia Pacific Microwave Conference*, vol. 2, pp. 621–624, Dec. 1997.

[80] H. Arai and K. Nakada, "Design parameters of proximity coupled taper slot antenna," *IEICE Technical Report*, AP98-18, pp. 9–16, June 1998 (in Japanese).

[81] M. Abramowitz and A. Stegun, eds. *Handbook of Mathematical Functions with Formulas, Graphs, and Mathematical Tables*, Dover 1964.

[82] B. Zhou, H. Li, and T. J. Cui, "Broadband and high-gain planar Vivaldi antennas based on inhomogeneous anisotropic zero-index metamaterial," *Progress in Electromagnetic Research*, vol. 120, 235-247, 2011.

[83] M. Sun, Z.N. Chen, and X. Qing, "Gain Enhancement of 60 GHz Antipodal Tapered Slot Antenna Using Zero-Index Metamaterial," *IEEE Transaction on Antennas and Propagation*, vol. 61, no. 4, pp. 1741-1746, April 2013.

[84] M. Bhaskar, E. Johari, Z. Akhter, and M. J. Akhtar, "Gain enhancement of the Vivaldi antenna with band notch characteristics using Zero-Index Metamaterial," *Microwave and optical technology Letters*, vol. 58, no.1, Jan. 2016.